Clays and Clay Minerals, Vol. 69, No. 1:94–104, 2021

PREPARATION AND CHARACTERIZATION OF HALLOYSITE-BASED CARRIERS FOR QUERCETIN LOADING AND RELEASE

Shu-Ting Liu[1]*, Xue-Gang Chen[2], Shi-Long Zhang[3], Xue-Min Liu[1], and Jun-Ji Zhang[1]

[1]Department of Geochemistry, Chengdu University of Technology, Chengdu 610059, China
[2]Ocean College, Zhejiang University, Zhoushan 316021, China
[3]School of Physics and Electronics, Qiannan Normal University for Nationalities, Duyun 558000, China

Abstract—Halloysite nanotubes (HNTs) have attracted much attention as delivery carriers for various drugs, but the loading of one such drug, quercetin, on HNTs has been investigated only rarely and usually involved cyclic vacuum pumping. The main objective of the present study was to develop a novel carrier system based on HNTs for quercetin delivery without a vacuum process and to investigate the effect of chemical modification of HNTs on the loading and release of quercetin. For this purpose, comparative studies of five chemical modification reagents (sodium lauroamphoacetate, cocoamidopropyl betaine, 1-hydroxyethyl 2-nonyl imidazoline betaine, triethanolamine, and dipicolinic acid) functionalized on HNTs were investigated for quercetin loading and in vitro release. Characterization of raw halloysite, modified halloysite, and quercetin-loaded halloysite were done by X-ray diffraction (XRD), Fourier-transform infrared spectrometry (FTIR), thermogravimetric analysis (TGA), and transmission electron microscopy (TEM). The results indicated that chemical modification could improve the interactions between HNTs and quercetin. After chemical modification, quercetin was anchored to both the inner and outer surfaces of HNTs by electrostatic attraction, hydrogen bonding, and van der Waals forces. Sodium lauroamphoacetate-modified HNTs were given the highest loading of 1.96 wt.% among the five reagents. Cocamidopropyl betaine-modified HNTs exhibited the best sustained-release profile with only 29.07% for initial burst release and 480 h of consecutive release. Carboxyl groups of the modification reagent improved the loading capacity of quercetin. Amide groups prolonged drug release due to the strong affinity between amine and phenolic hydroxyl groups of quercetin. The release of quercetin from the cocamidopropyl betaine-modified HNTs fitted a first-order kinetics model well. The present study suggested that cocamidopropyl betaine-modified HNTs offer promise as vehicles for delivery of quercetin and for extending the application of quercetin.

Keywords—Bioavailability · Drug release · Halloysite nanotubes · Quercetin · Surface modification

INTRODUCTION

Quercetin, a typical flavonoid, is produced naturally in the flowers, leaves, and fruits of plants, occurring mainly as a glycoside such as rutin, quercitrin, and hyperoside (Williamson and Manach 2005). With optimized numbers and distinctive positions of the free hydroxyl groups, quercetin (3,3′,4′,5,7-pentahydroxyflavone) has been reported extensively for its superior oxidation resistance and numerous pharmacological functions including anti-bacterial, anti-inflammatory, hypoglycemic, and anti-tumor properties (Kuo 1996; Hollman and Katan 1999; Kumari et al. 2010). Quercetin suffers low bioavailability, however, due to its poor aqueous solubility (7.7 μg/mL) and instability in physiological media (Guo et al. 2012; Pool et al. 2013). As a result, the clinical application and other practical uses of quercetin are restricted. In order to circumvent these problems, a wide variety of natural and synthetic polymer-delivery systems have been developed to encapsulate quercetin, including nano-emulsions, solid lipid nanoparticles, filled hydrogel particles, and more (Wang et al. 2016). Although the amounts of quercetin loaded in polymer-delivery systems can be significant, the initial rapid release from quercetin-loaded samples is still a critical problem.

Halloysite nanotubes (HNTs) are members of the kaolin group of clay minerals and crystallize typically as microtubules 1 μm long, the external and internal diameters range from 200–2000 and 100–700 Å, respectively. As a natural nanomaterial, the dimensions of HNTs depend largely on the geological environment which can lead to various features in terms of polydispersity, specific surface area, and rotational mobility (Cavallaro et al. 2018). Halloysite is a 1:1 layer aluminosilicate ($Al_2Si_2O_5(OH)_4{\cdot}2H_2O$). Chemically, the external surface of HNTs is composed of Si–O–Si groups, whereas the internal surface consists of a gibbsite-like array of Al–OH groups (Lisuzzo et al. 2019). Thus, HNTs exhibit the unique characteristic of possessing a positive charge on the internal surface and a negative charge on the external surface of the nanotubes when the pH is 2–8 (Vinokurov et al. 2017; Zeraatpishe et al. 2019). Pristine HNTs suggest high biocompatibility and low cytotoxicity, which suggests safe use in biological and medical fields (Santos et al. 2019; Vikulina et al. 2020). Moreover, the hollow tubular structure provides HNTs with a versatile, nanosized scaffold for drug delivery (Hanif et al. 2018). Drugs such as aspirin (Lun et al. 2014; Li et al. 2016), diphenhydramine hydrochloride, diclofenac sodium salt (Hemmatpour et al. 2015), ibuprofen (Tan et al. 2014), and doxorubicin (Lee et al. 2013) can be incorporated into HNTs via three different mechanisms: adsorption, intercalation, and tubular entrapment.

* E-mail address of corresponding author: liushuting@zju.edu.cn
DOI: 10.1007/s42860-021-00110-3

In recent years, several studies have referred to the use of raw and modified HNTs in quercetin-delivery systems. Employing the vacuum method, at <3.5 wt.% quercetin loading, most of the molecules are located within the pristine halloysite tubes (Hári et al. 2016). By grafting functionalized amphiphilic cyclodextrin onto outer surfaces of nanotubes, Massaro et al. (2015) showed that HNTs could be employed as simultaneous carriers for two different natural drugs, silibinin and quercetin, at 6.1% and 2.2% loadings, respectively. Furthermore, a synergic HNT-based nano-antioxidant was obtained by different functionalization of the external surface and the inner lumen of HNTs, in which Trolox was grafted selectively onto the HNT external surface; while quercetin was loaded into the inner lumen through vacuum cycling (Massaro et al. 2016). To date, quercetin delivery systems based on halloysite carriers have not been explored. In addition, most studies of halloysite-based carriers for drug loading have been conducted using cyclic vacuum pumping, which is a complex process.

In order to improve the drug-loading and release properties of halloysite-based carriers, modification methods such as covalent functionalization, non-covalent functionalization, selective etching, etc., have been applied generally on either or both external and internal surfaces of HNTs (Lazzara et al. 2018). The aim of the present study was to develop a novel carrier system for quercetin delivery based on HNTs and to identify the effect of chemical modification of HNTs in order to improve the quercetin loading capacity and release profile.

EXPERIMENTAL

Materials

The HNTs were supplied by the Yanbo mineral processing plant (Shijiazhuang, China). Three kinds of industrial-grade zwitterionic surfactant, including sodium lauroamphoacetate (S1), cocamidopropyl betaine (S2), and 1-hydroxyethyl 2-nonyl imidazoline betaine (S3), were purchased from Jinyu Chemical Co., Ltd (Shouguang, China). Dimethyl sulfoxide (DMSO), triethanolamine (TEOA), quercetin, and ethanol were obtained from Sinopharm Chemical Reagent Co., Ltd (Shanghai, China). Dipicolinic acid (DPA) was purchased from Aladdin Industrial Corporation (Shanghai, China). The structures of quercetin and of the modification reagents are shown in Fig. 1. All materials were used without further purification.

Surface Modification of HNTs

The HNTs were first preintercalated by DMSO, the methodology being revised from de Faria et al. (2009). Ten grams of halloysite was suspended in a mixture of 90 mL of DMSO and 10 mL of H_2O, which was maintained at 80°C under agitation for 5 days. The mixing material was centrifuged at 4000 rpm (maximum speed: 15000 rpm; tube dimensions: 38 mm×105 mm; angle: 25°) with a relative centrifugal force of 1755×*g* for 5 min. The resulting solid phase was washed with ethanol, and then oven-dried at 80°C.

The DMSO-preintercalated HNTs were named as H-DMSO. In a typical set of experiments (Letaief and Detellier 2007; Dedzo et al. 2012), 3 g of H-DMSO was dispersed in 18 g of S1, S2, S3, and TEOA, respectively. The mixtures were stirred at 110°C (S1, S2, and S3) and 180°C (TEOA) under nitrogen for 24 h at a speed of 200 rpm. After that, all mixtures were aged isothermally at 150°C for 24 h. The resulting materials were washed with 300 mL of distilled water to remove ungrafted compounds (de Faria et al. 2010) and dried in an oven at 60°C. They were designated as H-S1, H-S2, H-S3, and H-TEOA, respectively, according to the modification reagents.

In addition, modification of HNTs with DPA was also carried out. In a typical procedure, 10 g of DPA was first dispersed in 100 mL of ethanol and stirred for 30 min at 200 rpm. H-DMSO (2 g) was still used as a starting material and added to the DPA-ethanol solution. The mixture was stirred at 100°C under nitrogen for 24 h at a speed of 200 rpm. The resulting mixture was washed with ethanol three times (3×50 mL) and then stirred in 300 mL of distilled water for 24 h to remove the excess DPA. The material obtained was oven-dried at 60°C overnight and named as H-DPA.

Quercetin Loading

The method of soaking or equilibration was employed for quercetin loading. 0.6 g of each surface-modified HNT was suspended in 30 mL of 0.02 g·mL^{-1} quercetin in DMSO solution followed by stirring for 48 h at room temperature. The mixture was centrifuged at 4000 rpm (1755×*g*) for 5 min and dried in an oven at 60°C. The materials obtained after this process were denoted as H-TEOA-Q, H-DPA-Q, H-S1-Q, H-S2-Q, and H-S3-Q, respectively. The principal procedures of the surface modification of HNTs and of the drug-loading procedure are shown in Fig. 2.

Characterization

The HNT powder samples were placed in aluminum holders and characterized by X-ray diffraction (XRD). Diffraction patterns for each sample were collected at room temperature using a SHIMADZU XRD-6000 diffractometer (Hitachi Ltd, Tokyo, Japan) with CuKα (λ = 0.15406 nm) radiation from 3–80°2θ with a scan step of 0.02°2θ. The operation voltage and current were maintained at 40 kV and 40 mA, respectively. The FTIR spectra of the samples were recorded using a Bruker VERTEX 70 spectrometer (Bruker Corporation, Billerica, Massachusetts, USA) at a resolution of 4 cm^{-1} and a range of 4000–400 cm^{-1} using the KBr/HNTs pellet technique at a ratio of 100:1. Thermogravimetric analyses (TG) were performed using a Q500 TA Instrument (TA Instruments Inc, New Castle, Delaware, USA) under a nitrogen flow of 60 mL min^{-1} for the sample and of 40 mL min^{-1} for the balance. The finely ground sample was introduced into a ceramic crucible and placed in the furnace along with the reference sample. The weight of each sample was ~5 mg. Measurements were carried out by heating the sample from 50 to 900°C at a rate of 10°C min^{-1}. The micro-morphologies of the samples were studied using a JEM-2010 (JEOL Ltd, Tokyo, Japan) high-resolution transmission electron microscope (HR-TEM) with an accelerating voltage of 200 kV and

https://doi.org/10.1007/s42860-021-00110-3 Published online by Cambridge University Press

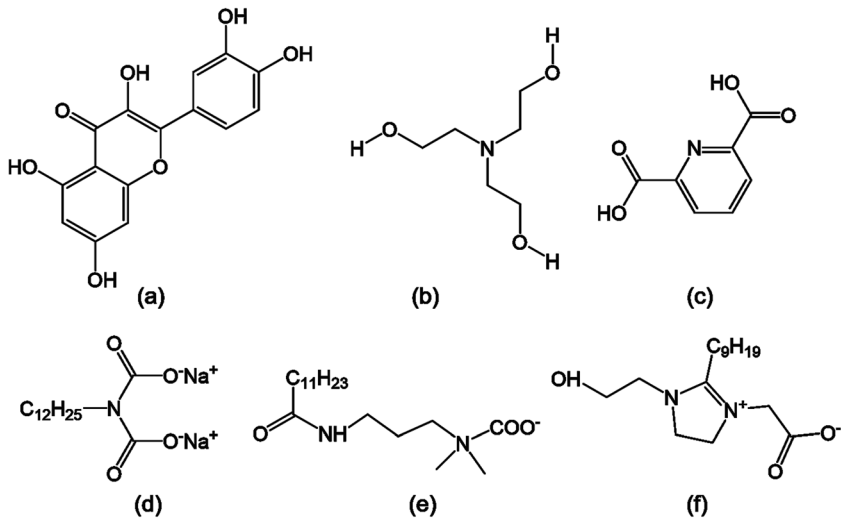

Fig. 1. Chemical structures of **a** quercetin and of modification reagents: **b** Triethanolamine, **c** Dipicolinic acid, **d** Sodium lauroamphoacetate, **e** Cocamidopropyl betaine, and **f** 1-hydroxyethyl 2-nonyl imidazoline betaine

a point resolution of 1.9 nm. The powder samples were suspended in ethanol, deposited drop-wise, and evaporated on 200 mesh copper grids covered with amorphous Formvar carbon.

In vitro Release Study

In vitro release of quercetin from quercetin-loaded HNTs was undertaken by the dialysis bag method (Dian et al. 2014; Zhang et al. 2020). Briefly, 10 mg of quercetin-loaded HNTs was encapsulated in a dialysis bag (molecular weight cut off 8000–14,000 Da) with 3 L of ethanol. The dialysis bag was suspended in 30 mL of the same medium. The whole system was then placed in a thermostatic shaking water bath at 37°C and stirred at 100 rpm. At given time intervals, 3 mL of the incubated medium was withdrawn for testing and replenished with the equivalent volume of fresh medium. The quercetin concentration was determined by UV-Vis absorbance at λ_{max} of 374 nm by a SHIMADZU UV-2550 UV/VIS spectrophotometer (Hitachi Ltd, Tokyo, Japan). The release tests were repeated three times to obtain the average results with standard errors.

RESULTS AND DISCUSSION

Structure and Characterization

The structural characteristics of raw and modified HNTs were revealed in XRD patterns (Fig. 3a). The XRD trace of raw halloysite contained a set of peaks at 12.1, 20.1, 24.6, 35.0, 54.5, and 62.6°2θ, which were indexed as 7 Å halloysite (JCPDF#29-1487). The additional peak at 8.8°2θ is characteristic of 10 Å halloysite. Both the 7.3 and 10 Å phases were observed, indicating that the raw HNTs were partially dehydrated (Du et al. 2010). The intercalation of surface-modifying reagents or drugs may result in an increase in the basal spacing (d_{001}). In the present case, DMSO was first pre-intercalated into the interlayer spaces, causing an expansion of the basal spacing to 11.2 Å, which is consistent with previous reports (Bobos et al. 2001; Franco and Cruz 2002). With consecutive steps of replacement intercalation, H-DMSO was used as a precursor for further surface modification, although this was not always accompanied by an increase in d_{001}. In fact, after treatments with S1, S2, S3, and DPA the basal spacing of halloysite reverted to 7.3 Å. Meanwhile, the d_{001} reflection became less intense, whereas the peaks in the range

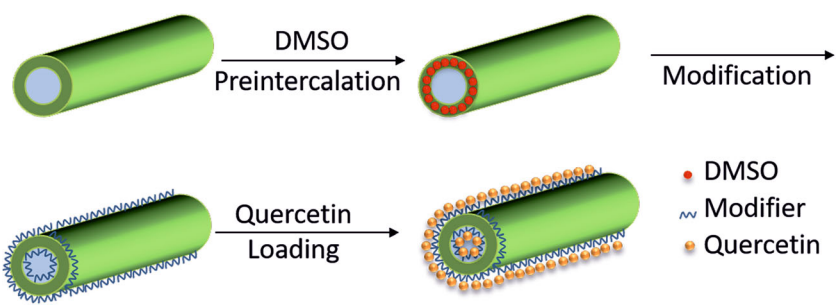

Fig. 2. Schematic illustration of surface modification of HNTs and the drug-loading procedure

https://doi.org/10.1007/s42860-021-00110-3 Published online by Cambridge University Press

of ~20–30°2θ were still sharp and clear. The results indicated that the halloysite crystal order was disturbed, but only along the *c* axis not the *a* and *b* axes. That was because during the S1, S2, S3, and DPA treatments the high temperature and washing led to deintercalation of DMSO (Frost and Kloprogge 1999; Yariv and Lapides 2008; Zhang et al. 2011). Intercalation and deintercalation influenced significantly the parallel arrangement of the layers along the *c* axis, which was in accordance with earlier studies (Wada 1961; Matusik et al. 2009). The interlayer space of H-TEOA reached a value of 11.1 Å, which was consistent with earlier reports (Letaief and Detellier 2007; Letaief et al. 2008; Matusik and Wścisło 2014). Because the d_{001} value of H-DMSO was 11.2 Å (very close to the observed d_{001} value of H-TEOA), the XRD patterns are not unequivocal evidence that DMSO was replaced by TEOA (Letaief and Detellier 2007). The surface-modified HNTs maintained a d_{001} spacing of 11.2 Å after quercetin loading, i.e. with no further increase (Fig. 3b). This indicated that the expansion of d_{001} was due to the intercalation of DMSO during the drug-loading process while the quercetin did not intercalate into the interlamellar space of HNTs. The characteristic reflection of quercetin was not detected in the XRD patterns of drug-loaded composites, which may be due to the small loading amount of quercetin or due to the fact that the quercetin was adsorbed onto HNTs only in the amorphous form (Hári et al. 2016). According to Pool et al. (2013), compared to crystalline quercetin, quercetin in amorphous form is more bioavailable, which is desirable for delivery systems designed for use in pharmaceuticals or functional foods.

In the FTIR spectra of raw and modified HNTs (Fig. 4a), the absorption bands at 3620, 3697, and 3456 cm^{-1} were assigned to the O–H stretching vibrations of: (1) structural hydroxyl groups of the octahedral sheet at the inner plane where the tetrahedral and octahedral sheets are joined, denoted inner hydroxyl groups; (2) hydroxyl groups located at the outer plane of the octahedral sheet, denoted inner-surface hydroxyl groups; and (3) the hydrogen bond between interlayer water and inner-surface hydroxyl groups, respectively (Kodama and Oinuma 1963; Zhang et al. 2015). The –OH deformation vibrations of adsorbed water provided a broad signal at 1632 cm^{-1} (Zich et al. 2013). The bands at 1096 cm^{-1} and 1031 cm^{-1} were ascribed to the in-plane stretching vibration of the Si–O network (Si–O–Si and O–Si–O), whereas the 754 and 692 cm^{-1} bands were derived from the perpendicular Si–O stretching vibration (Zich et al. 2013; Zhang et al. 2013, 2017). The presence of the band at 910 cm^{-1} corresponded to the deformation vibrations associated with the Al–OH groups (Frost and Shurvell 1997). After intercalation with DMSO, the obvious peak at 3697 cm^{-1} disappeared and, instead, three smaller peaks appeared at 3659, 3537, and 3502 cm^{-1}. These peaks were assigned to hydrogen bonds between intercalated DMSO molecules and inner-surface hydroxyl groups of HNTs (S=O–HO) (Avila et al. 2010). The C–H stretching bands observed in the FTIR spectra in the 3000–2800 cm^{-1} region due to the grafted organic molecules from modification regents were distinctive in H-S1, H-S2, H-S3, and H-DPA. Combined with the XRD results, the d_{001} spacing of H-S1, H-S2, H-S3, and H-DPA remaining at 7.3 Å indicated that these modification agents were grafted on the inner and external surfaces rather than intercalating the interlayer space. Furthermore, the deintercalation of DMSO caused by the grafting process of S1, S2, S3, and DPA was also illustrated by the reappearance of the peak at 3697 cm^{-1} and the absence of the characteristic bands of DMSO at 3659, 3537, and 3502 cm^{-1}.

In the case of H-TEOA, the presence of grafted TEOA was confirmed by the C–H stretching vibration peaks at 2918 and 2850 cm^{-1}. A decrease in intensity of the hydroxyl groups at 3621 and 3698 cm^{-1} was observed in the H-TEOA spectrum, accompanied by the disappearance of the DMSO signal. These results indicated that DMSO was replaced by TEOA. The corresponding XRD analysis revealed the d_{001} value of H-TEOA to still be 11.1 Å, however. DMSO in the interlayer was replaced by TEOA, therefore. Meanwhile, the peak at 3697 cm^{-1} in H-TEOA was weak but still sharp and clear, which meant the replacement of DMSO by TEOA was incomplete and some interlayer hydroxyls were not bonded with TEOA. Additionally, an obvious increase in peak intensity at 3453 cm^{-1} was assigned to co-intercalated water in the interlayer space during the intercalation of TEOA.

The FTIR spectra of quercetin (Fig. 4b) displays a relatively broad phenolic OH band centered around 3400 cm^{-1}, –CO stretching at 1665 cm^{-1}, and aromatic bending and stretching around 1100 and 1600 cm^{-1} (Natarajan et al. 2011). For the FTIR spectra of the quercetin-loaded HNTs, the intensities of the inner-surface hydroxyl groups and outer-surface hydroxyl groups at 3620 and 3697 cm^{-1} decreased with a slight red shift around 3453 cm^{-1}, while the peak intensity at 1085 and 1034 cm^{-1} increased. Based on the XRD and FTIR results, quercetin was adsorbed on the surface or in the inner lumen of HNTs due to hydrogen bonding between the surface hydroxyl groups and quercetin molecules, rather than intercalation into the interlayers of the HNTs.

Microstructural Analysis

The TEM image of pristine HNTs (Fig. 5) exhibits a cylindrical shape with hollow and open-ended tubular morphology. Two regions of different transparencies corresponded to the walls with greater opacity and tube lumen space of HNTs with greater transparency. Quercetin-loaded HNTs were different from pristine halloysite in having more opaque lumens as seen in the TEM images of H-TEOA-Q, H-DPA-Q, H-S1-Q, H-S2-Q, and H-S3-Q, indicating that grafted modification agents and quercetin almost filled the hollow lumen of the HNTs. The encapsulation of quercetin in the lumen of HNTs is driven by capillary and surface-tension forces (Mei et al. 2011). Some precipitate also appeared on the external surfaces of the HNTs, which was much rougher than the external surfaces of pristine HNTs and modified HNTs as seen in Fig. 6. The external precipitate may be due to hydrogen bonding or Van der Waals forces between the outer surface hydroxyl group or the siloxane group of the HNTs and quercetin (Aguzzi et al. 2007), or the grafted modification reagents may have provided more effective adsorption sites for quercetin molecules.

https://doi.org/10.1007/s42860-021-00110-3 Published online by Cambridge University Press

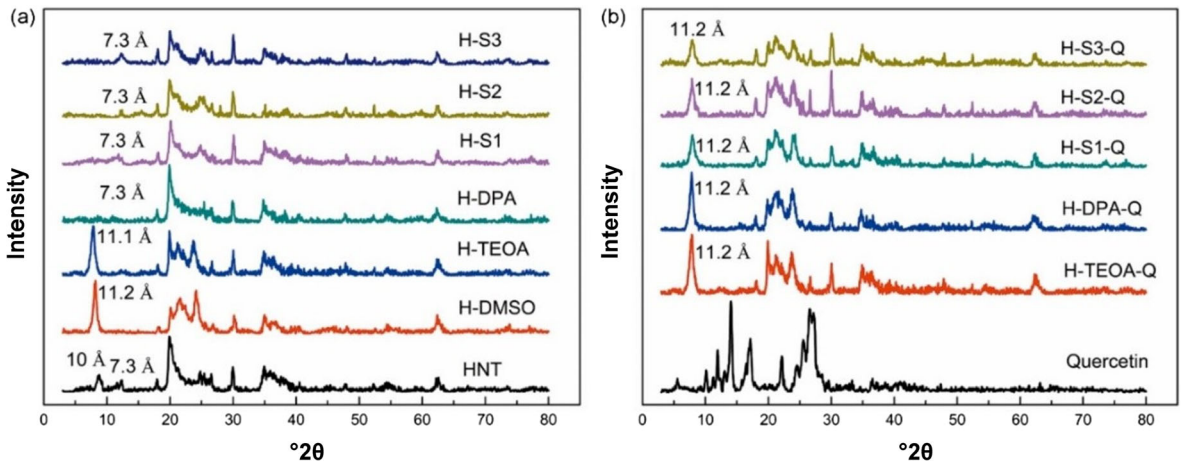

Fig. 3. XRD patterns of **a** surface-modified HNTs and **b** quercetin-loaded HNTs

Thermal Behavior

Thermogravimetry and differential thermogravimetric analyses (TGA-DTG) were done to evaluate the thermal stability of quercetin, raw HNTs, modified HNTs, and quercetin-loaded HNTs. The TGA/DTG curves of raw halloysite (Fig. 7) revealed two distinct weight-loss stages. The first mass loss occurred in the range 300–550°C with a loss of 9.0 wt.% and the endothermic peak at 473°C, which is ascribed to the dehydroxylation of structural inner hydroxyls (Panda et al. 2010). The second DTG peak with a minor weight loss of 2.9 wt.% centered at ~723°C may be attributed to the decomposition of mineral impurities such as calcite (Li et al. 2017; Ben Salah et al. 2018). The presence of calcite can be verified by its typical peak located at ~30°2θ (*hkl* = 104) according to the XRD pattern. The residual mass of raw halloysite retained ~84.0 wt.% at 900°C. After modification, additional weight loss below 400°C was exhibited in the TGA/DTG curves of modified HNTs (Fig. 7a,c) with three or four mass-loss stages; the amounts of char residue of modified HNTs were less than those of raw halloysite at 900°C, however. Specifically, for H-DMSO, the first weight loss of 11.9 wt.% occurred in the range 100–280°C with the DTA peak at 179°C and may have resulted from the evaporation of DMSO molecules. Two weight-loss steps centered at 468 and 743°C with weight losses of 7.1 wt.% and 2.2 wt.% followed; these were assigned to loss of structural inner hydroxyls and decomposition of calcite (Karunadasa et al. 2019), respectively.

In the TGA/DTA pattern of H-TEOA, three major stages of mass loss were detected. The first weight loss (1.5 wt.%), which occurred from ~50 to 150°C with a DTG peak at 97°C, was associated with physically adsorbed water. The second weight loss (9.7 wt.%), in the range 300–400°C with a broad DTG peak, corresponded to the decomposition of TEOA, which was grafted onto Al–OH groups (Letaief and Detellier 2007). The third DTG peak at 418°C, with weight loss of 4.6 wt.%, which accounted for the dehydroxylation of the clay mineral, shifted significantly to a lower temperature than that of raw halloysite, H-DMSO, and other modified HNTs. This result was consistent with previous reports that the dehydroxylation temperature of halloysite intercalated with various compounds is lower than that of raw halloysite in varying degrees, according to various intercalation agents

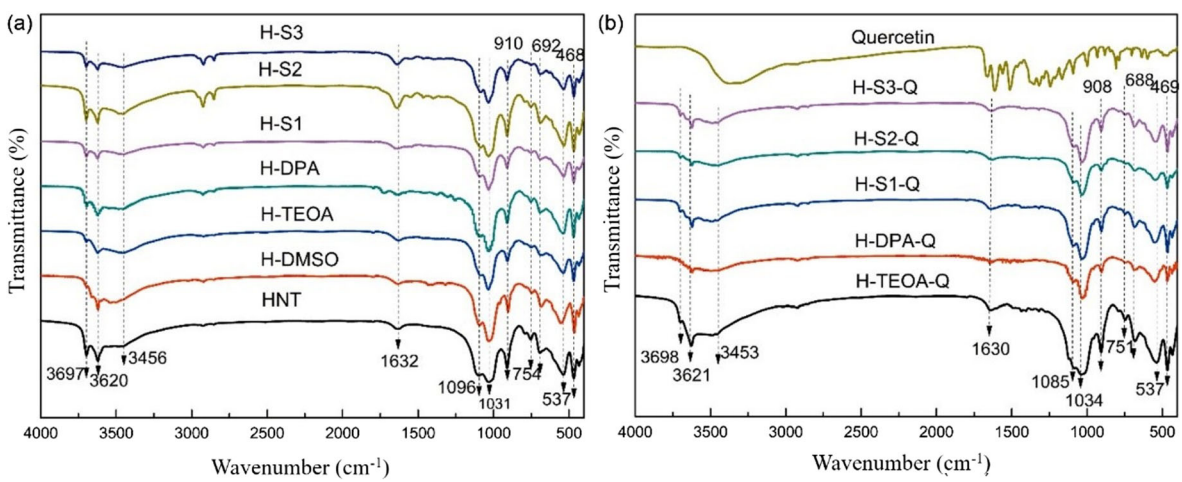

Fig. 4. FTIR spectra of quercetin, raw HNTs, modified HNTs, and quercetin-loaded HNTs

https://doi.org/10.1007/s42860-021-00110-3 Published online by Cambridge University Press

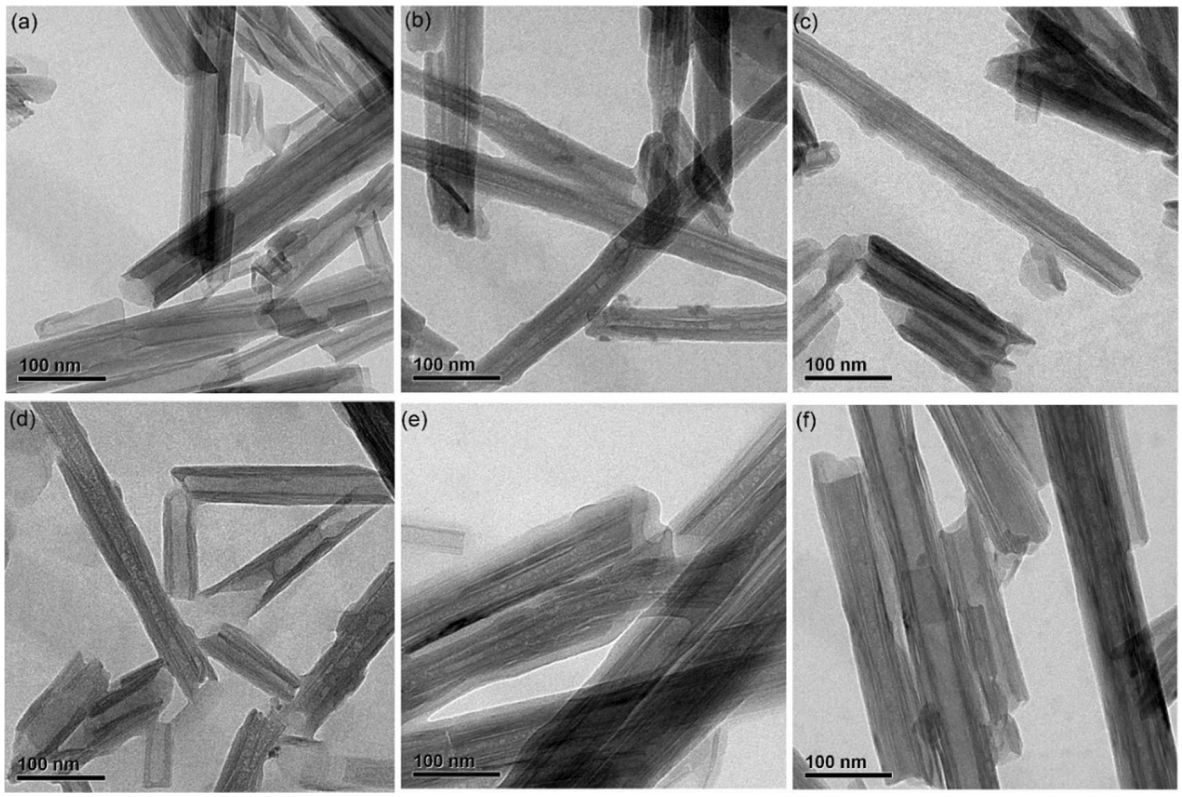

Fig. 5. TEM images of **a** HNTs, **b** H-TEOA-Q, **c** H-DPA-Q, **d** H-S1-Q, **e** H-S2-Q, and **f** H-S3-Q

(Cheng et al. 2010; Seifi et al. 2016; Zhou et al. 2018). Intercalation molecules expand the interlayer spacing, thus weakening the hydrogen bonds between adjacent halloysite layers and bringing about easier surface dehydroxylation (Zhou et al. 2018). The mass loss of organic compounds which occurred at 279, 258, and 259°C was observed in H-S1, H-S2, and H-S3, respectively, while HNTs displayed no corresponding peaks in the 200–300°C temperature range. This result confirmed the analyses by XRD and FTIR that the S1, S2, and S3 molecules were grafted onto the external and internal surfaces of the halloysite nanotubes. The char values of H-S1, H-S2, and H-S3 decreased to 77.31, 70.72, and 68.15 wt.%, respectively.

In order to obtain a better understanding of the degradation events ascribed to the presence of quercetin, the quercetin was also submitted to thermal analysis. The TGA/DTG curves of quercetin (Fig. 8) illustrated that a maximum mass loss at 340°C corresponded to its thermal decomposition. According to the results of XRD, DMSO became intercalated into the interlayer space during the quercetin loading process, thus the DTG curves of H-S1-Q, H-S2-Q, and H-S3-Q displayed a similar pattern to that of H-DMSO with a mass loss in the range 100–300°C, which was ascribed to the elimination of intercalated DMSO. Two similar, but higher-intensity, DTG peaks occurred at 275 and 296°C for H-DPA-Q and H-TEOA-Q, respectively, suggesting a lower decomposition temperature and faster weight loss of the grafting agent. Although the characteristic thermal decomposition peak of quercetin at 340°C was not clear in the TGA/DTG curves of quercetin-loaded HNTs, the DSC and TGA curves of loaded and non-loaded HNTs were different, especially at <300°C, providing evidence of the interaction of quercetin with the modifiers (Pereira et al. 2020). The TGA curve of quercetin-loaded HNTs underwent a continued weight loss in the first weight-loss step (~10.7, 16.6, 14.6, 10.7, and 10.7 wt.% for H-TEOA-Q, H-S1-Q, H-DPA-Q, H-S2-Q, and H-S3-Q, respectively), which was ascribed to the dehydration and thermal decomposition of HNTs and quercetin. Because the quercetin might be loaded as an amorphous form, its thermogravimetric performance might be different, with decomposition shifting towards a lower temperature than that of pure quercetin in crystalline form. The DSC curve of H-TEOA-Q, H-S1-Q, H-DPA-Q, H-S2-Q, and H-S3-Q presented endothermic peaks at ~270–300°C, which were assigned to the melting point of quercetin (Qi et al. 2015).

Release Profile

The extended release profiles of quercetin from the H-TEOA-Q, H-DPA-Q, H-S1-Q, H-S2-Q, and H-S3-Q samples (Fig. 9) exhibited a two-stage release behavior, including a fast-linear release and a subsequent prolonged release. The release percentage after 24 h of drug-loaded HNTs (Table 1) was noted to decrease in the following order H-S3-Q > H-DPA-Q > H-TEOA-Q > H- S1-Q > H-S2-Q, and the time required for the rate of drug release to plateau (equilibrium time) from H-TEOA-Q, H-DPA-Q, H-S1-Q, H-S2-Q, and H-S3-Q was 240, 288, 480, 480, and 192 h,

https://doi.org/10.1007/s42860-021-00110-3 Published online by Cambridge University Press

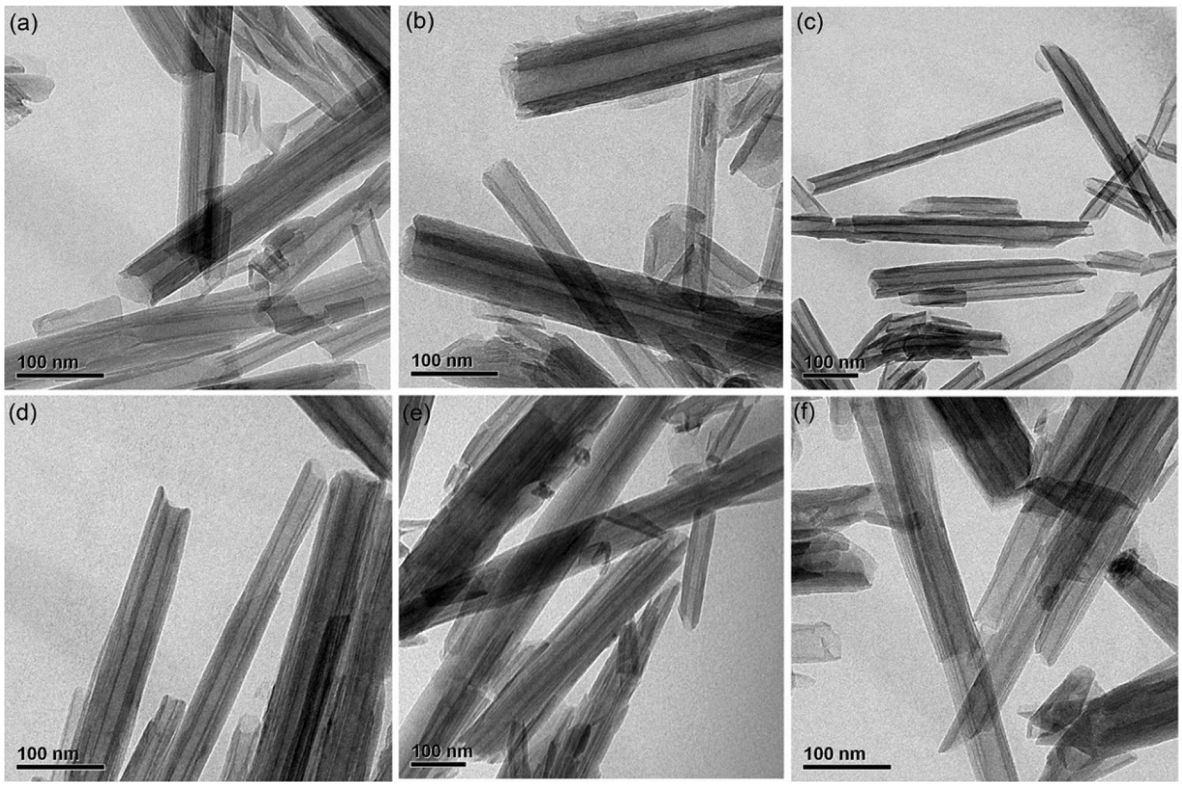

Fig. 6. TEM images of **a** HNTs, **b** H-TEOA, **c** H-DPA, **d** H-S1, **e** H-S2, and **f** H-S3

respectively. This result confirmed that the surface-modification treatment had affected significantly the drug-loading and -release properties. In particular, H-S2-Q displayed a sustained-release profile, with only 29.07% for the initial burst release and 480 h for subsequent release. This quercetin-release rate of H-S2-Q is slower than that of the halloysite compound reported previously (Massaro et al. 2015). The favorable release properties of H-S2-Q could be due to the active amide and carboxyl groups of S2, which could provide more effective adsorption sites and strengthen the interaction between quercetin and H-S2. Both carboxyl and amide groups of modifiers introduced more hydrogen-binding sites and, thus, enhanced the retention of quercetin, which is prone to form H-bonds (Wang et al. 2013). H-DPA-Q had the greatest loading content of 1.96 wt.%, followed by H-S1-Q (Table 1). According to the molecular structure of these surfactants, DPA and S1 have two carboxyl groups, which means that they are highly polar. This molecular structure (containing two carboxyl groups) facilitates drug loading through hydrogen bonding, electrostatic attraction, and Van der Waals forces. The phenolic hydroxyl groups of quercetin could form stronger electrostatic interaction with the amide groups of S1 and S2 than with the carboxyl groups, however. Hydrogen bonding between amide and hydroxyl groups also enhanced quercetin stability, resulting in a more prolonged release (Xia et al. 2006; Lee et al. 2008).

Because cyclic vacuum pumping was not applied in the present study, however, the loading efficiency of modified HNTs was limited; quercetin can still be anchored on modified HNTs through interaction with the grafted surfactants by means of electrostatic attraction, hydrogen bonding, and Van der Waals forces. The selective interaction which occurs between quercetin and functional groups of surfactants, such as the carboxyl groups, could increase quercetin loading, while amide groups enhance drug stability and prolong drug action. Overall, the results suggested that the H-S2-Q sample could be a potential material for applications in drug storage and delivery.

Release Kinetics

In order to study further the release behavior of quercetin from HNTs, the in vitro release data were fitted to first-order and Higuichi theoretical kinetics models to analyze the kinetics and the release mechanism of quercetin, using the expressions.

$$\text{First-order equation: } M_t/M_\infty = 1-e^{-k_1 t} \quad (1)$$

$$\text{Higuchi's model: } M_t/M_\infty = k_H\, t^{1/2} \quad (2)$$

In these models, M_t is the amount of drug released at time t; M_∞ is the cumulative mass of drug released; k_1 and k_H are the release constants of the respective equations; t is the release time; and n is the diffusion

https://doi.org/10.1007/s42860-021-00110-3 Published online by Cambridge University Press

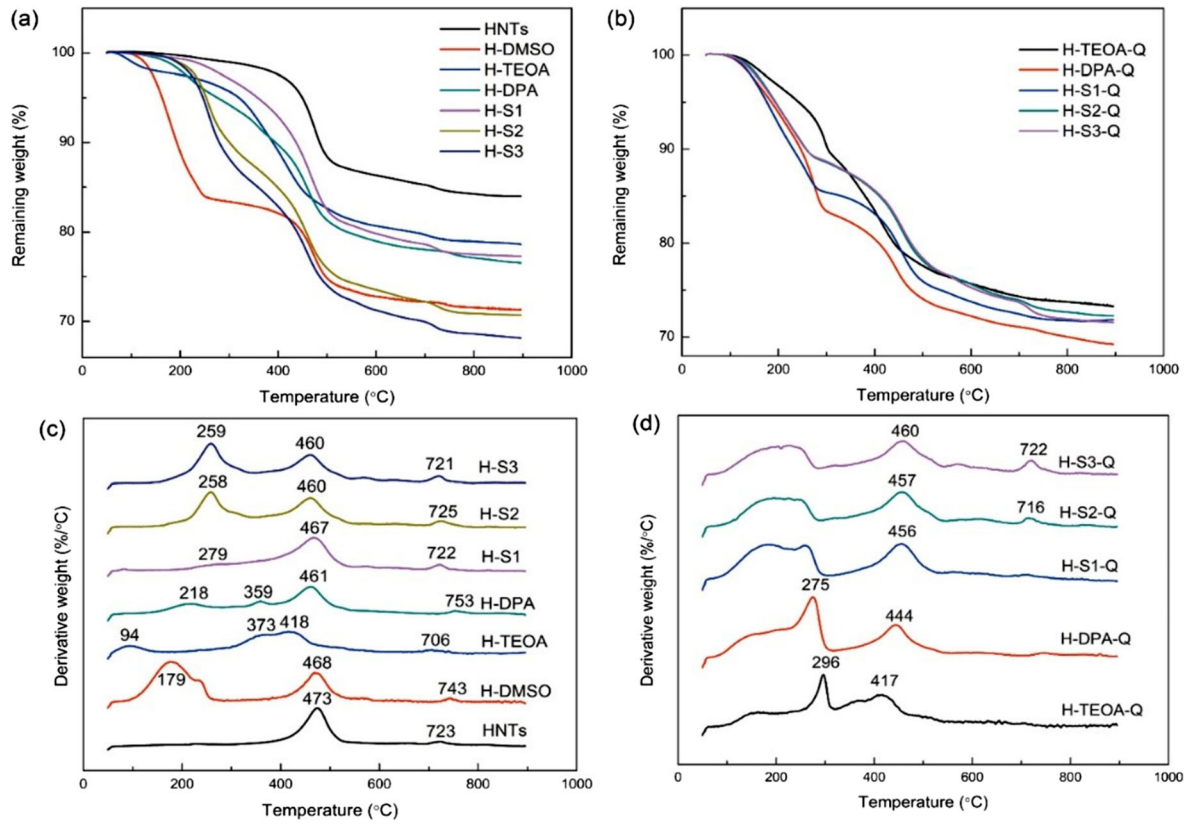

Fig. 7. TGA and DTG curves of H-DMSO and of pristine, modified, and quercetin-loaded HNTs

exponent, which is a characteristic of the release mechanism. The correlation coefficient (R^2) and the release parameter values are reported in Table 2. Because the release profiles of H-TEOA-Q, H-DPA-Q, H-S1-Q, and H-S3-Q consisted of an initial burst release within 24 h and a subsequent slow drug release, these two stages based on release rate were fitted separately to the various models. Two stages of drug release behavior on halloysite were also reported by previous studies, which suggested that drug molecules contained inside the nanotube lumen undergo a slow diffusion process while externally adsorbed molecules undergo a fast desorption (Aguzzi et al. 2013). The first-order release kinetics suggested a concentration-dependent process. The Higuchi model interpreted the rate of drug release from a matrix where the drug loading exceeds its solubility in the matrix into a surrounding solution (Paul 2011). In this case, the release kinetic studies show that a first-order equation is appropriate to describe the release process of quercetin from H-DPA-Q and H-S2-Q, while the Higuchi model fitted

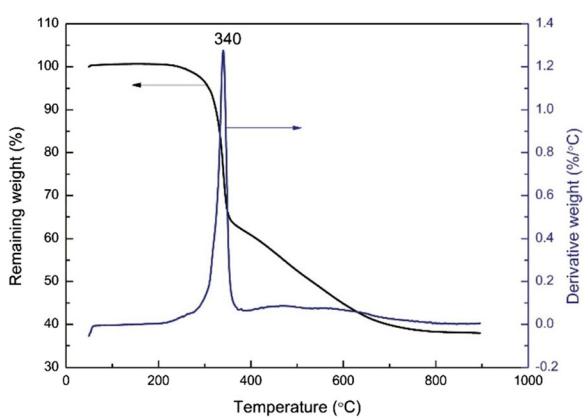

Fig. 8. TGA-DTG curves of quercetin

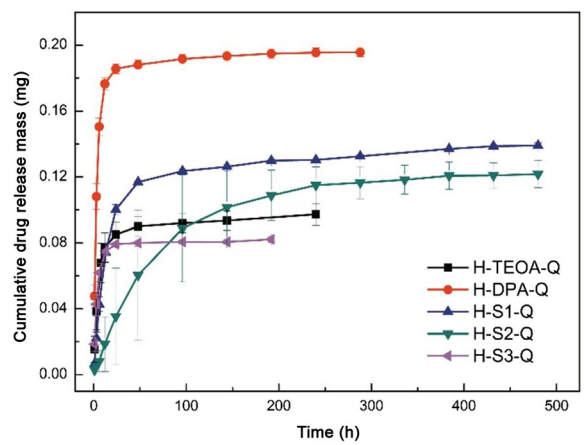

Fig. 9. Release profiles of quercetin from H-TEOA-Q, H-DPA-Q, H-S1-Q, H-S2-Q, and H-S3-Q

https://doi.org/10.1007/s42860-021-00110-3 Published online by Cambridge University Press

Table 1. The release properties of quercetin-loaded HNTs

Sample	Release percentage after 24 h (%)	Equilibrium time (h)	Actual drug loading (wt.%)
H-TEOA-Q	87.47	240	0.97
H-DPA-Q	94.91	288	1.96
H-S1-Q	72.01	480	1.39
H-S2-Q	29.07	480	1.22
H-S3-Q	96.46	192	0.82

better for H-TEOA-Q, H-S1-Q, and H-S3-Q. This result revealed that the quercetin release process from H-TEOA-Q, H-S1-Q, and H-S3-Q is controlled mainly by diffusion, while for H-DPA-Q and H-S2-Q, quercetin release depends on its concentration. In addition, the first-order release constant (k_1) of H-S2-Q at the first stage (0.012) was relatively small, resulting in a desirable prolonged release. For H-TEOA-Q, H-S1-Q, and H-S3-Q, the rate of release of the quercetin into the surrounding fluid was governed by Fick's law of diffusion. While the concentration gradient decreased as more quercetin was released into the surrounding media, the diffusion rate decreased and in turn affected the release rate.

CONCLUSIONS

The HNTs were functionalized with five chemical reagents for efficient drug loading and release. Quercetin was anchored to both the inner and outer surfaces of HNTs by covalent interactions and hydrogen bonding. The carboxyl and amide groups of the modifiers introduced hydrogen-binding sites and, thus, enhanced the retention of quercetin, which is prone to forming H-bonds. Cocamidopropyl betaine was the most effective modification reagent for HNTs in this study. The release of quercetin from the cocamidopropyl betaine-modified HNTs fitted well with the first-order kinetics model. This quercetin-loaded HNTs system not only significantly prolonged the release of the quercetin, but also reduced appreciably the initial burst release from the antioxidant nanomaterial. The modified HNTs were useful for incorporating quercetin into the lumen and contributed to improving the bioavailability of quercetin. This system, as developed, should be efficient for applications in sustained drug delivery and pharmaceutical sciences.

Table 2. Parameters of fitting models of quercetin-loaded HNTs

Sample	Model	k		R^2	
H-TEOA-Q	Higuchi	–26.172	–1.079	0.9779	0.9309
H-DPA-Q	First-order	0.183	0.018	0.9700	0.9470
H-S1-Q	Higuchi	–17.733	–1.035	0.9942	0.9811
H-S2-Q	First-order	0.012		0.9909	
H-S3-Q	Higuchi	–26.065	–0.334	0.9070	0.8273

ACKNOWLEDGMENTS

This work was supported by the Science and Technology Department of Sichuan Province under Grant 18YYJC1029 and National Science Foundation for Young Scientists of China under Grant 41603044. The authors thank the State Key Laboratory of Chemical Engineering in Zhejiang University for assistance in testing and analyzing the samples.

Declarations

Conflict of Interest

The authors declare that they have no conflict of interest.

Funding

Funding sources are as stated in the Acknowledgments.

REFERENCES

Aguzzi, C., Cerezo, P., Viseras, C., & Caramella, C. (2007). Use of clays as drug delivery systems: Possibilities and limitations. *Applied Clay Science, 36*, 22–36.

Aguzzi, C., Viseras, C., Cerezo, P., Salcedo, I., Sanchez-Espejo, R., & Valenzuela, C. (2013). Release kinetics of 5-aminosalicylic acid from halloysite. *Colloids Surface B: Biointerfaces, 105*, 75–80.

Avila, L. R., de Faria, E. H., Ciuffi, K. J., Nassar, E. J., Calefi, P. S., Vicente, M. A., & Trujillano, R. (2010). New synthesis strategies for effective functionalization of kaolinite and saponite with silylating agents. *Journal of Colloid and Interface Science, 341*, 186–193.

Ben Salah, I., Sdiri, A., Ben M'barek Jemai, M., & Boughdiri, M. (2018). Potential use of the Lower Cretaceous clay (Kef area, northwestern Tunisia). as raw material to supply ceramic industry. *Applied Clay Science, 161*, 151–162.

Bobos, I., Duplay, J., Rocha, J., & Gomes, C. (2001). Kaolinite to halloysite-7 Å transformation in the kaolin deposit of São Vicente de Pereira, Portugal. *Clays and Clay Minerals, 49*, 596–607.

Cavallaro, G., Chiappisi, L., Pasbakhsh, P., Gradzielski, M., & Lazzara, G. (2018). A structural comparison of halloysite nanotubes of different origin by small-angle neutron scattering (SANS) and electric birefringence. *Applied Clay Science, 160*, 71–80.

Cheng, H., Liu, Q., Yang, J., Zhang, J., & Frost, R. L. (2010). Thermal analysis and infrared emission spectroscopic study of halloysite–potassium acetate intercalation compound. *Thermochimica Acta, 511*, 124–128.

de Faria, E. H., Lima, O. J., Ciuffi, K. J., Nassar, E. J., Vicente, M. A., Trujillano, R., & Calefi, P. S. (2009). Hybrid materials prepared by interlayer functionalization of kaolinite with pyridine-carboxylic acids. *Journal of Colloid and Interface Science, 335*, 210–215.

de Faria, E. H., Ciuffi, K. J., Nassar, E. J., Vicente, M. A., Trujillano, R., & Calefi, P. S. (2010). Novel reactive amino-compound: Tris(hydroxymethyl)aminomethane covalently grafted on kaolinite. *Applied Clay Science, 48*, 516–521.

https://doi.org/10.1007/s42860-021-00110-3 Published online by Cambridge University Press

Dedzo, G. K., Letaief, S., & Detellier, C. (2012). Kaolinite-ionic liquid nanohybrid materials as electrochemical sensors for size-selective detection anions. *Journal of Materials Chemistry,* ***22***, 20593–20601.

Dian, L. H., Yu, E. J., Chen, X. N., Wen, X. G., Zhang, Z. Z., Qin, L. Z., Wang, Q. Q., Li, G., & Wu, C. B. (2014). Enhancing oral bioavailability of quercetin using novel soluplus polymeric micelles. *Nanoscale Research Letters, 9*, 684–695.

Du, M., Guo, B., & Jia, D. (2010). Newly emerging applications of halloysite nanotubes: A review. *Polymer International, 59*, 574–582.

Franco, F., & Cruz, M. D. R. (2002). High-temperature X-ray diffraction, differential thermal analysis and thermogravimetry of the kaolinite-dimethylsulfoxide intercalation complex. *Clays and Clay Minerals, 50*, 47–55.

Frost, R. L., & Kloprogge, J. T. (1999). Raman spectroscopy of the low-frequency region of kaolinite at 298 and 77 K. *Applied Spectroscopy, 53*, 1610–1616.

Frost, R. L., & Shurvell, H. F. (1997). Raman microprobe spectroscopy of halloysite. *Clays and Clay Minerals, 45*, 68–72.

Guo, C., Yang, C., Li, Q., Tan, Q., Xi, Y., Liu, W., & Zhai, G. (2012). Development of a quercetin-loaded nanostructured lipid carrier formulation for topical delivery. *International Journal of Pharmaceutics, 430*, 292–298.

Hanif, M., Jabbar, F., Sharif, S., Abbas, G., Farooq, A., & Aziz, M. (2018). Halloysite nanotubes as a new drug-delivery system: A review. *Clay Minerals, 51*, 469–477.

Hári, J., Polyák, P., Mester, D., Mičušík, M., Omastová, M., Kállay, M., & Pukánszky, B. (2016). Adsorption of an active molecule on the surface of halloysite for controlled release application: Interaction, orientation, consequences. *Applied Clay Science, 132–133*, 167–174.

Hemmatpour, H., Haddadi-Asl, V., & Roghani-Mamaqani, H. (2015). Synthesis of pH-sensitive poly (N,N-dimethylaminoethyl methacrylate)-grafted halloysite nanotubes for adsorption and controlled release of DPH and DS drugs. *Polymer, 65*, 143–153.

Hollman, P. C., & Katan, M. B. (1999). Dietary flavonoids: Intake, health effects and bioavailability. *Food and Chemical Toxicology, 37*, 937–942.

Karunadasa, K. S. P., Manoratne, C. H., Pitawala, H. M. T. G. A., & Rajapakse, R. M. G. (2019). Thermal decomposition of calcium carbonate (calcite polymorph). as examined by in-situ high-temperature X-ray powder diffraction. *Journal of Physics and Chemistry of Solids, 134*, 21–28.

Kodama, H., & Oinuma, K. (1963). Identification of kaolin minerals in the presence of chlorite by X-ray diffraction and infra-red adsorption spectra. *Clays and Clay Minerals, 11*, 236–249.

Kumari, A., Yadav, S. K., Pakade, Y. B., Singh, B., & Yadav, S. C. (2010). Development of biodegradable nanoparticles for delivery of quercetin. *Colloids and Surfaces B: Biointerfaces, 80*, 184–192.

Kuo, S. M. (1996). Antiproliferative potency of structurally distinct dietary flavonoids on human colon cancer cells. *Cancer Letters, 110*, 41–48.

Lazzara, G., Cavallaro, G., Panchal, A., Fakhrullin, R., Stavitskaya, A., Vinokurov, V., & Lvov, Y. (2018). An assembly of organic-inorganic composites using halloysite clay nanotubes. *Current Opinion in Colloid & Interface Science, 35*, 42–50.

Lee, K. W., Kang, N. J., Heo, Y. S., Rogozin, E. A., Pugliese, A., Hwang, M. K., Bowden, G. T., Bode, A. M., Lee, H. J., & Dong, Z. (2008). Raf and mek protein kinases are direct molecular targets for the chemopreventive effect of quercetin, a major flavonol in red wine. *Cancer Research, 68*, 946–955.

Lee, Y., Jung, G. E., Cho, S. J., Geckeler, K. E., & Fuchs, H. (2013). Cellular interactions of doxorubicin-loaded DNA-modified halloysite nanotubes. *Nanoscale, 5*, 8577–8585.

Letaief, S., & Detellier, C. (2007). Functionalized nanohybrid materials obtained from the interlayer grafting of aminoalcohols on kaolinite. *Chemical Communications, 25*, 2613–2615.

Letaief, S., Tonle, I. K., Diaco, T., & Detellier, C. (2008). Nanohybrid materials from interlayer functionalization of kaolinite. Application to the electrochemical preconcentration of cyanide. *Applied Clay Science, 42*, 95–101.

Li, X., Yang, Q., Ouyang, J., Yang, H., & Chang, S. (2016). Chitosan modified halloysite nanotubes as emerging porous microspheres for drug carrier. *Applied Clay Science, 126*, 306–312.

Li, Y., Zhang, Y., Zhang, Y., Liu, M., Zhang, F., & Wang, L. (2017). Thermal behavior analysis of halloysite selected from Inner Mongolia autonomous region in China. *Journal of Thermal Analysis and Calorimetry, 129*, 1333–1339.

Lisuzzo, L., Cavallaro, G., Milioto, S., & Lazzara, G. (2019). Layered composite based on halloysite and natural polymers: A carrier for the ph controlled release of drugs. *New Journal of Chemistry, 43*, 10887–10893.

Lun, H., Ouyang, J., & Yang, H. (2014). Natural halloysite nanotubes modified as an aspirin carrier. *RSC Advances, 4*, 44197–44202.

Massaro, M., Piana, S., Colletti, C. G., Noto, R., Riela, S., Baiamonte, C., Giordano, C., Pizzolanti, G., Cavallaro, G., Milioto, S., & Lazzara, G. (2015). Multicavity halloysite–amphiphilic cyclodextrin hybrids for co-delivery of natural drugs into thyroid cancer cells. *Journal of Materials Chemistry B, 3*, 4074–4081.

Massaro, M., Riela, S., Guernelli, S., Parisi, F., Lazzara, G., Baschieri, A., Valgimigli, L., & Amorati, R. (2016). A synergic nanoantioxidant based on covalently modified halloysite-trolox nanotubes with intra-lumen loaded quercetin. *Journal of Materials Chemistry B, 4*, 2229–2241.

Matusik, J., & Wścisło, A. (2014). Enhanced heavy metal adsorption on functionalized nanotubular halloysite interlayer grafted with aminoalcohols. *Applied Clay Science, 100*, 50–59.

Matusik, J., Gaweł, A., Bielańska, E., Osuch, W., & Bahranowski, K. (2009). The effect of structural order on nanotubes derived from kaolin-group minerals. *Clays and Clay Minerals, 57*, 452–464.

Mei, D., Zhang, B., Liu, R., Zhang, H., & Liu, J. (2011). Preparation of stearic acid/halloysite nanotube composite as form-stable pcm for thermal energy storage. *International Journal of Energy Research, 35*, 828–834.

Natarajan, V., Krithica, N., Madhan, B., & Sehgal, P. K. (2011). Formulation and evaluation of quercetin polycaprolactone microspheres for the treatment of rheumatoid arthritis. *Journal of Pharmaceutical Sciences, 100*, 195–205.

Panda, A. K., Mishra, B. G., Mishra, D. K., & Singh, R. K. (2010). Effect of sulphuric acid treatment on the physico-chemical characteristics of kaolin clay. *Colloids and Surfaces A: Physicochemical and Engineering Aspects, 363*, 98–104.

Paul, D. R. (2011). Elaborations on the higuchi model for drug delivery. *International Journal of Pharmaceutics, 418*, 13–17.

Pereira, A. B., Silva, A. M.d., Barroca, M. J., Marques, M. P. M., & Braga, S. S. (2020). Physicochemical properties, antioxidant action and practical application in fresh cheese of the solid inclusion compound γ-cyclodextrin·quercetin, in comparison with β-cyclodextrin·quercetin. *Arabian Journal of Chemistry, 13*, 205–215.

Pool, H., Mendoza, S., Xiao, H., & McClements, D. J. (2013). Encapsulation and release of hydrophobic bioactive components in nanoemulsion-based delivery systems: Impact of physical form on quercetin bioaccessibility. *Food & Function, 4*, 162–174.

Qi, Y., Jiang, M., Cui, Y.-L., Zhao, L., & Zhou, X. (2015). Synthesis of quercetin loaded nanoparticles based on alginate for Pb(II) adsorption in aqueous solution. *Nanoscale Research Letters, 10*, 1–9.

Santos, A. C., Pereira, I., Reis, S., Veiga, F., Saleh, M., & Lvov, Y. (2019). Biomedical potential of clay nanotube formulations and their toxicity assessment. *Expert Opinion on Drug Delivery, 16*, 1169–1182.

Seifi, S., Diatta-Dieme, M. T., Blanchart, P., Lecomte-Nana, G. L., Kobor, D., & Petit, S. (2016). Kaolin intercalated by urea. Ceramic applications. *Construction and Building Materials, 113*, 579–585.

Tan, D., Yuan, P., Annabi-Bergaya, F., Liu, D., Wang, L., Liu, H., & He, H. (2014). Loading and in vitro release of ibuprofen in tubular halloysite. *Applied Clay Science, 96*, 50–55.

Vikulina, A., Voronin, D., Fakhrullin, R., Vinokurov, V., & Volodkin, D. (2020). Naturally derived nano- and micro-drug delivery

vehicles: Halloysite, vaterite and nanocellulose. *New Journal of Chemistry, 44*, 5638–5655.

Vinokurov, V. A., Stavitskaya, A. V., Chudakov, Y. A., Ivanov, E. V., Shrestha, L. K., Ariga, K., Darrat, Y. A., & Lvov, Y. M. (2017). Formation of metal clusters in halloysite clay nanotubes. *Science and Technology of Advanced Materials, 18*, 147–151.

Wada, K. (1961). Lattice expansion of kaolin minerals by treatment with potassium acetate. *American Mineralogist, 46*, 78–91.

Wang, C. S., Liu, P., & Yu, N. (2013). Site-preference of uracil and thymine hydrogen bonding to quercetin. *Acta Physico-Chimica Sinica, 29*, 1173–1182.

Wang, W., Sun, C., Mao, L., Ma, P., Liu, F., Yang, J., & Gao, Y. (2016). The biological activities, chemical stability, metabolism and delivery systems of quercetin: A review. *Trends in Food Science & Technology, 56*, 21–38.

Williamson, G., & Manach, C. (2005). Bioavailability and bioefficacy of polyphenols in humans. Ii. Review of 93 intervention studies. *The American Journal of Clinical Nutrition, 81*, 243S–255S.

Xia, Y.-q., Guo, T.-y., Song, M.-d., Zhang, B.-h., & Zhang, B.-l. (2006). Selective separation of quercetin by molecular imprinting using chitosan beads as functional matrix. *Reactive and Functional Polymers, 66*, 1734–1740.

Yariv, S., & Lapides, I. (2008). Thermo-infrared-spectroscopy analysis of dimethylsulfoxide-kaolinite intercalation complexes. *Journal of Thermal Analysis and Calorimetry, 94*, 433–440.

Zeraatpishe, L., Mohebali, A., & Abdouss, M. (2019). Fabrication and characterization of biocompatible ph responsive halloysite nanotubes grafted with sodium alginate for sustained release of phenytoin sodium. *New Journal of Chemistry, 43*, 10523–10530.

Zhang, Y., Liu, Q., Wu, Z., Zheng, Q., & Cheng, H. (2011). Thermal behavior analysis of kaolinite–dimethylsulfoxide intercalation complex. *Journal of Thermal Analysis and Calorimetry, 110*, 1167–1172.

Zhang, Y., He, X., Ouyang, J., & Yang, H. (2013). Palladium nanoparticles deposited on silanized halloysite nanotubes: Synthesis, characterization and enhanced catalytic property. *Scientific Reports, 3*, 1–6.

Zhang, H., Ren, T., Ji, Y., Han, L., Wu, Y., Song, H., Bai, L., & Ba, X. (2015). Selective modification of halloysite nanotubes with 1-pyrenylboronic acid: A novel fluorescence probe with highly selective and sensitive response to hyperoxide. *ACS Applied Materials & Interfaces, 7*, 23805–23811.

Zhang, A., Mu, B., Luo, Z., & Wang, A. (2017). Bright blue halloysite/$CoAl_2O_4$ hybrid pigments: Preparation, characterization and application in water-based painting. *Dyes and Pigments, 139*, 473–481.

Zhang, R., Li, Y., He, Y., & Qin, D. (2020). Preparation of iodopropynyl butycarbamate loaded halloysite and its anti-mildew activity. *Journal of Materials Research and Technology, 9*, 10148–10156.

Zhou, Y., Liu, Q., Xu, P., Cheng, H., & Liu, Q. (2018). Molecular structure and decomposition kinetics of kaolinite/alkylamine intercalation compounds. *Frontiers in Chemistry, 6*, 310.

Zich, D., Zacher, T., Darmo, J., Szöcs, V., Lorenc, D., & Janek, M. (2013). Far-infrared investigation of kaolinite and halloysite intercalates using terahertz time-domain spectroscopy. *Vibrational Spectroscopy, 69*, 1–7.

(Received 2 May 2020; revised 6 January 2021; AE: F. Javier Huertas)